Comparison of double-pass estimates of the retinal-image quality obtained with green and near-infrared light

Norberto López-Gil and Pablo Artal

Laboratorio de Optica, Departamento de Física, Universidad de Murcia, Campus de Espinardo, Edificio C, 30071 Murcia, Spain

Received July 15, 1996; revised manuscript received November 5, 1996; accepted November 20, 1996

We compared retinal point-spread functions obtained by the double-pass method with two different wavelengths, green (543 nm) and near-infrared (780 nm), in both cases under the best conditions of focus. The best refractive state at each wavelength was determined with two procedures: subjective refraction and analysis of the recorded double-pass images as a function of focus. Since the refraction results agree quite well, we assume that in both cases, green and near-infrared light, most of the light of the central core in the double-pass images comes from a layer close to that of the photoreceptors. The central spread of the double-pass images was also quite similar for the two wavelengths: a width of ~2–3 arcmin at half-intensity relative to the peak. However, larger differences were found in the tails of the images, with the infrared images presenting a larger scattering halo, probably as a result of a more important contribution of retinal and choroidal scattering for that wavelength. By using the central core in the double-pass images and ignoring the tails, we can use the near-infrared data to predict the modulation transfer function measured with the use of green light. These results raise the possibility of using near-infrared illumination in the double-pass method to estimate the optical performance of the human eye. [S0740-3232(97)00305-0]

1. INTRODUCTION

The size and shape of the near-infrared retinal point-spread function plays a fundamental role in different widely used ophthalmic instruments and techniques, in particular, in infrared automatic refractors,[1] photorefraction devices,[2] infrared scanning laser ophthalmoscopes,[3] and optical coherence tomography.[4,5] The near-infrared line-spread function has been traditionally assumed to be largely more extended than the visible one. Cornsweet and Crane,[1] when developing an infrared optometer, suggested that for a 900-nm light, the line spread on the retina was very much broader than for visible light of the order of 1 deg of arc. Since then, this has been the typical view on the size of the near-infrared retinal spread function. A related problem is the characteristic of the retinal reflection for the infrared compared with the visible light. Whereas in the green–red range there is evidence that the effective surface for reflection and subjective refraction are nearly coincident,[6] in the near-infrared the effective reflecting surface is assumed to lie behind the photoreceptor plane.[7] In this context, it seems necessary to perform new measurements of the retinal spread function in near-infrared light.

An additional motivation for exploring the near-infrared optical image quality in the eye is the possibility of using an infrared double-pass apparatus to estimate the retinal image quality in visible light. The double-pass technique has been used during recent years to measure the optical performance of the eye, mainly through the ocular modulation transfer function[8–10] (MTF). In the method, the MTF is calculated from images of a point source recorded after reflection in the retina and double pass through the eye. Initially, monochromatic double-pass measurements were obtained with red He–Ne lasers (632 nm). Recently Williams *et al.*[6] showed that slightly better double-pass estimates of retinal-image quality are obtained in 543-nm rather than in 632-nm light. This is probably due to the higher retinal scattering for longer wavelengths. A potential limitation in the double-pass technique is the need to use relatively high levels of intensity of visible light during the measurements. This means that to obtain accurate results, subjects should have the pupil dilated and the accommodation paralyzed. This avoids pupil vignetting or large changes in the accommodation response that could mask the results. However, some interesting problems to be investigated, for instance the relationship between ocular aberrations and accommodation, require measurement of ocular optical performance under natural viewing. In addition, the use of near-infrared illumination would allow estimation of the retinal image quality more comfortably for the subject under natural conditions, thus leading to clinically oriented double-pass apparatus for ophthalmic optics testing, optometry, and ophthalmology. These are additional reasons to explore the potential of near-infrared illumination in the double-pass apparatus.

In this paper we evaluate the possibilities of using near-infrared illumination in the double-pass technique. We use a new apparatus allowing us to record double-pass images of green (543 nm) and near-infrared (780 nm) point sources under exactly the same optical conditions. We have chosen a near-infrared wavelength (780 nm)

0740-3232/97/050961-11$10.00

that is still slightly visible, allowing us to obtain subjective refraction data to complement the objective double-pass results.

2. METHODS

A. Green–Near-Infrared Double-Pass Apparatus

Figure 1 shows a schematic diagram of the double-pass apparatus used in the study. It is similar to that described in previous studies[8,10] but uses two pinholes, PH_1 and PH_2, 25 and 15-μm in diameter, respectively, that act as the point sources in green (543 nm), O_1, and near-infrared (780 nm) light, O_2. The green light comes from a He–Ne laser (Melles Griot 05 LGR 193) and the near-infrared from a diode laser (Spindler and Hoyer DL 25). The infrared beam is radially symmetric after spatial filtering. A removable mirror, RM, permits selection of the desired wavelength. Light coming either from O_1 or from O_2 is collimated by the achromatic doublet L_2 (f'_2 = 200 mm) and passes through the aperture P_1, which acts as the stop for the first pass. The light is reflected by the pellicle beam splitter (BS_1), passes through an achromatic Badal system [lenses L_3 and L_4 ($f'_3 = f'_4$ = 100 mm)], and a trial lens, TL, before reaching the eye. The subject's spherical refractive state is modified by moving backward and forward the block B containing lenses L_4, TL, and the eye. A CCD video camera (Sony AVC-D5CE) monitors the eye pupil through a second pellicle, BS_2 when the eye is illuminated with a 950-nm LED. This permits alignment of the eye pupil along the optical axis of the measuring setup. The light coming from the point source and reflected in the retina passes through lenses TL, L_4, L_3, and the aperture P_2 (stop of the second pass), forming the aerial (double-pass) image, which is collected by a scientific-grade cooled CCD camera (Spectra Source MCD 1000). The chromatic difference in focus of the whole system for the two wavelengths was measured. It comes mainly from the camera zoom objective, CZ. For each wavelength it was compensated by a small change in the focus setting to obtain the best-focused image with a plane mirror in place of the eye. The emission of the diode laser as a function of wavelength was also measured;

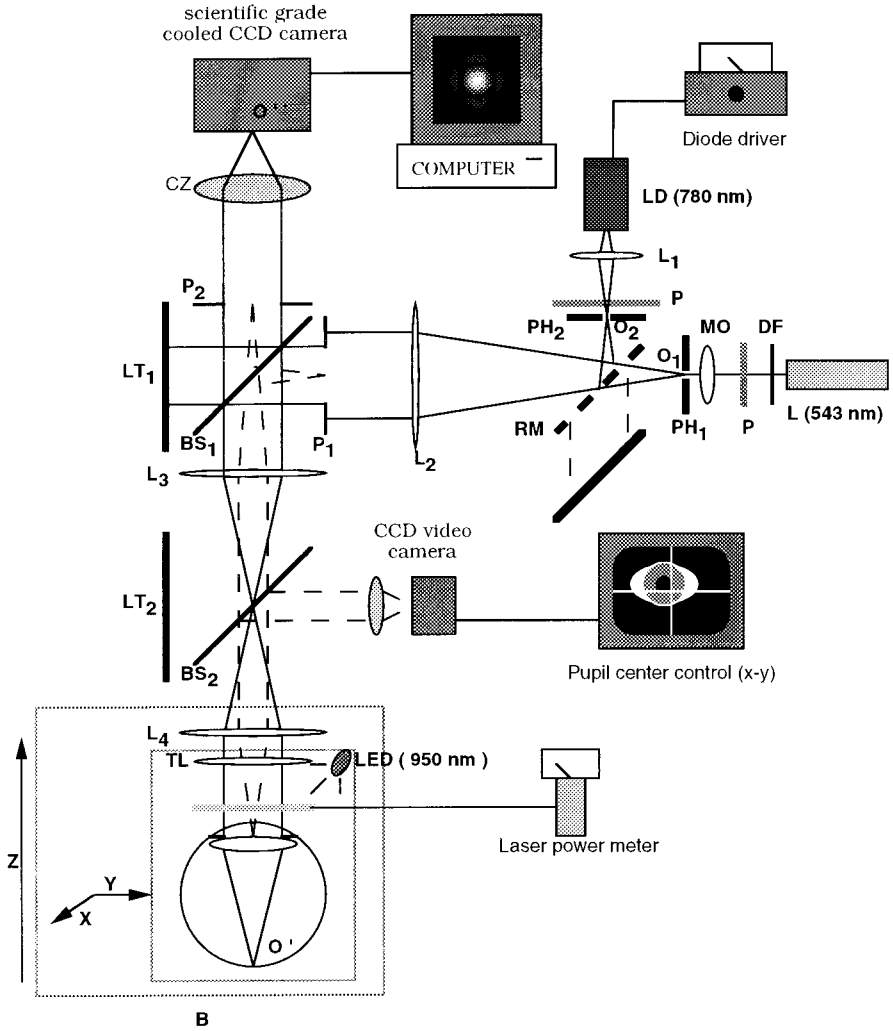

Fig. 1. Schematic diagram of the dual green–near-infrared double-pass apparatus. L, He–Ne laser (543 nm); LD, diode laser (780 nm); DF, neutral-density filter; P, linear polarizer; MO, microscope objective; PH1 and PH2, pinholes; L1, aspheric lens; RM, removable mirror; L3 and L4 achromatic doublets; P1 and P2, first- and second-pass stops; BS1 and BS2, pellicle beam splitters; TL, trial lens; LT1 and LT2, light trappers; CZ, camera zoom objective.

the peak emission was found to be 784 nm, and the width at half-height was smaller than 4 nm under the low-intensity conditions of use. The maximum irradiance on the cornea during exposures was less than 100 nW/cm^2 for both wavelengths. This is several orders of magnitude below the maximum permissible exposure limit (ANSI Z136.1; 1993).

B. Experimental Procedure

Three subjects were tested in the study: NL (male), CG (female), and PA (male); 27, 25, and 34 years old, respectively, myopic with normal vision and best corrected decimal acuity 1 or better (see Table 1 below for exact refractive errors). For subject NL, three different complete sets of data were collected, NL1–3, over a period of two months. Accommodation was paralyzed with two drops of tropycamide (1%) instilled 5 min apart, except in the case of NL2, in which two drops of cyclopentholate (1%) were used. No significant difference was found in the results of subjects NL with the two types of drug. The subject's head was fixated by means of a bite bar mounted on a three-axis positioner stage used to align the natural pupil with respect to the projected artificial pupil. All the data were collected in foveal vision, and the measurement object point source served as the fixation target.

In the first part of the experiment, the best refractive state for each wavelength was precisely determined. We refracted the eye for each wavelength with two different procedures. Subjects looked for the best focus by moving the block B while viewing the point source directly, and the intensity was conveniently attenuated with neutral-density filters. This task can also be performed in the infrared because 780-nm light is still slightly visible. The subjects were instructed to change the relative distance between the block B and lens L_3 (Fig. 1), to see the smallest and the brightest point source. For each wavelength, five subjective settings were taken and the average and the standard deviation calculated. Second, to obtain the refractive state objectively, series of double-pass images were recorded for different focus positions 0.2 diopters (D) or less apart around the point of subjective best focus. Two image-quality parameters were computed from each double-pass image, assuming that the best image in terms of optical quality would correspond to the subject's best focus. The parameters were (1) the normalized maximum intensity divided by the mean intensity value of each image and (2) the Strehl ratio[11] calculated as the volume under the two-dimensional MTF divided by the volume under the diffraction-limited MTF for that pupil diameter.

Once the best refractive state for each wavelength had been found, a complete collection of double-pass images was obtained. We recorded 16-bit images at the selected best refractive state for each wavelength with 4-mm-diameter-stop entrance and exit sizes. Time exposure was 5 s, which was long enough to break the coherence in the second pass and short enough to avoid large eye movements and ensure the comfort of the observer. For each condition, four double-pass images and one background image were recorded. Series of images with two different sizes of the field of view were collected: 256 $\times$ 256-pixel images corresponding to 79.4 arcmin with a sampling rate of 0.31 arcmin per pixel (with 300-mm focal length in the camera zoom objective, CZ) and 512 $\times$ 512-pixel images corresponding to 476 arcmin with a sampling rate 0.93 arcmin per pixel (with 100-mm focal length in CZ). This allowed us to compare in detail the green and the infrared aerial images both at their central cores and at the wide-angle tails of the images. A background image (acquired without the eye in the system) was subtracted from the average of four double-pass images. This allowed us to remove the CCD bias, scattered light from the system, and possible artifacts.

Additional series of double pass-images were collected with a configuration in the double pass with different-size entrance and exit pupil diameters, as previously reported.[10] This version of the double-pass apparatus permits us to obtain full information on the ocular asymmetric aberrations that otherwise are canceled in the second passage.[12]

C. Modulation Transfer Function

The MTF is computed as the square root of the modulus of the Fourier transformation of the average double-pass image captured with equal-size entrance and exit pupil diameters. A peak appears at zero frequency in the modulus of the Fourier transform of the retinal images because of the dc offset in the double-pass images produced by ocular and retinal scattering, light out of focus coming from deeper layers,[3] corneal reflex, and light coming from the setup that has not been eliminated. Since the zero spatial frequency in the Fourier domain is normalized to value 1, all values at frequencies different from zero are reduced. Two procedures have previously been proposed to overcome this limitation when the MTF is calculated from double-pass retinal images[8,10,13]: (1) subtracting a constant background veil in the double-pass image before computing the Fourier transform and (2) removing all the values in the MTF at spatial frequencies lower than 3 cycles per (c/deg) degree.[10] We applied the latter procedure, in which the missing values in the transfer function are extrapolated with use of an exponential function[9] and the MTF is recalculated by dividing the function by the extrapolated value at zero spatial frequency. Finally, we calculated the average value in the MTF for spatial frequencies larger than the diffraction-limit value. Since the actual MTF should be zero for these spatial frequencies, we subtract that value and renormalize to obtain the MTF. In the case of subsampled images with spatial-frequency values at the edge of the window in the Fourier domain lower than the diffraction limit, we subtract the average value obtained in the last five pixels at the edge of the window.

3. RESULTS

A. Subjective and Double-Pass Refractive States for 543 and 780 nm

Figure 2(a) shows a series of double-pass images obtained in subject PA (entrance and exit aperture 4 mm) for the green wavelength with different focus positions. In Fig. 2(b) two image-quality parameters, the maximum in the image divided by the mean normalized irradiance and the Strehl ratio, computed for each image are plotted as a

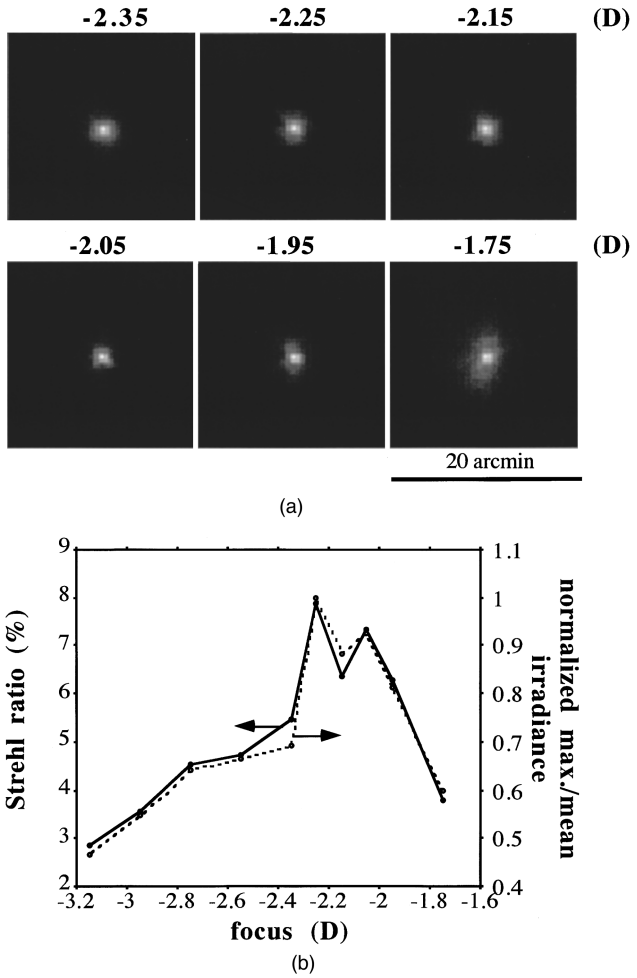

Fig. 2. (a) Double-pass aerial images for observer PA in different foci with green light and 4-mm pupil diameter in both passes. (b) Two different image-quality criteria used to select the best image: the Strehl ratio (solid curve) and the normalized maximum divided by the mean irradiance (dashed curve) as a function of focus.

function of focus. Figure 3(a) presents the series of double-pass images, and Fig. 3(b) plots the image-quality parameters as a function of focus for the near-infrared wavelength in subject PA. Figures 4 and 5 show the same results in subject CG for green and near-infrared light, respectively. The double-pass image in each series with the higher value of the image-quality parameters is selected as the best double-pass focus to estimate the objective refractive state. Table 1 presents a summary of the subjective and the double-pass best focus at each wavelength and the chromatic difference of focus between the two wavelengths. Similar double-pass and subjective values of refraction appear for the two wavelengths, except for observer PA in green, for which a 0.35-D difference was found. The standard deviation of the subjective data was lower than 0.2 D in all the cases, being slightly higher for green than for near-infrared light. The chromatic difference in focus between 543 and 780 nm was ~1 D. Each change of 1 mm in the relative position of block B produces a difference in focus of 0.1 D that corresponds approximately to 37.9 μm of axial shift in the retina. According to the results of Table 1, the average distance found between the subjective and the objective focal planes in the retina for both the near-infrared and green light is 0.1 D or lower. This would correspond in both cases to a distance between subjective and objective focus smaller than 40 μm, around one half the length of a foveal cone. These results extend to the near-infrared range the previous findings obtained with a similar procedure in red light (632 nm).[6] This also suggests that the double-pass setup captures most of the infrared light as well as the green light that forms the central peak of the image from a retinal layer close to that of the photoreceptors.

B. Double-Pass Images with Equal Entrance and Exit Pupil Diameters

Double-pass retinal images for 543 and 780 nm for the three subjects were obtained with the conventional configuration of the apparatus with equal-size entrance and exit pupils of 4-mm diameter. Images with two different sizes of field of view were collected each time by changing the magnification and the full size of the image. Figure 6 shows the normalized intensity of the radial averaging

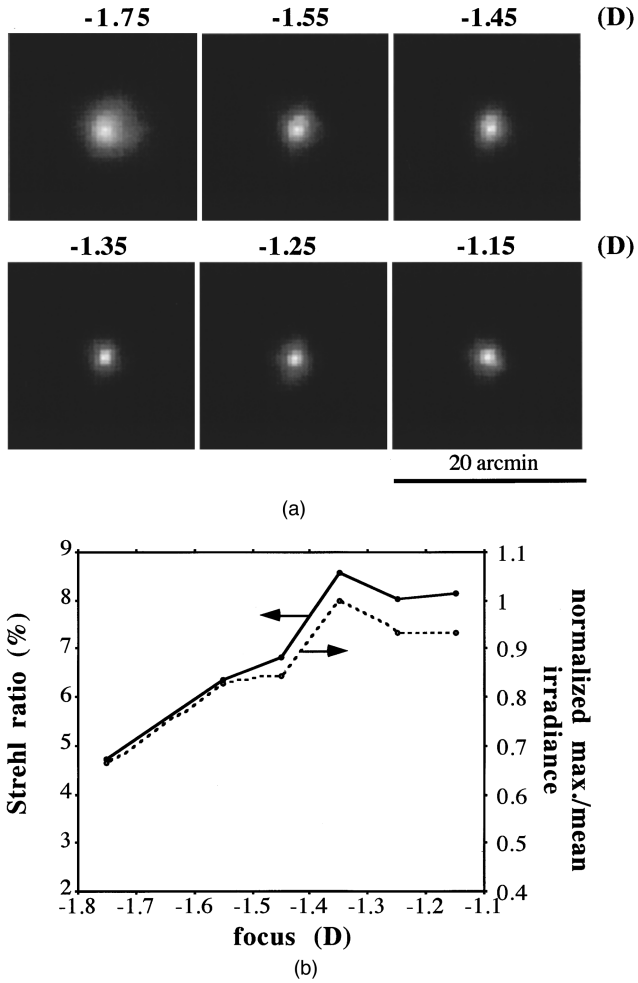

Fig. 3. (a) Double-pass aerial images for observer PA in different foci with near-infrared light and 4-mm pupil diameter in both passes. (b) Two different image-quality criteria used to select the best image: the Strehl ratio (solid curve) and the normalized maximum divided by the mean irradiance (dashed curve) as a function of focus.

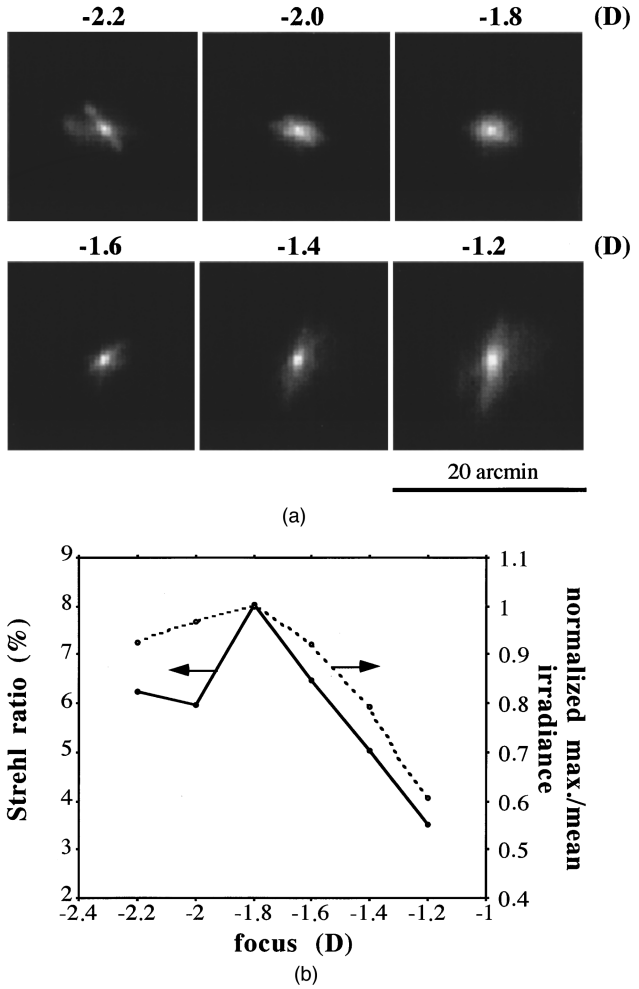

Fig. 4. (a) Double-pass aerial images for observer CG in different foci when using green light and 4-mm pupil diameter in both passes. (b) Two different image-quality criteria used to select the best image: the Strehl ratio (solid curve) and the normalized maximum divided by the mean irradiance (dotted curve) as a function of focus.

across all directions for subjects (a) NL3 and (b) PA in the high-magnification double-pass images. These results show the differences in the central cores of the images. Figure 7 shows the normalized-intensity (radial-profile) images obtained for the same subjects under exactly the same experimental conditions with low magnification. The intensity axis of the curves corresponding to the large-field-of-view images are plotted with a logarithmic intensity scale to allow a better comparison. The central parts of the images are relatively similar, with the infrared slightly more spread. However, larger differences are found in the tails of the images. The large-field-of-view curves in Fig. 7 show clearly that the intensity in the green images is close to the ground level (~0.001 in the normalized scale) beyond approximately 1 deg. However, the near-infrared curves are considerably higher for larger angles and keep falling up to 3 deg of visual angle. These results confirm the expected larger retinal scattering and also probably that light out of focus is coming from deeper layers for infrared light. We calculated the area under the double-pass images up to 2 deg for both near-infrared and green. The ratio of these two values can be used as an index of the different amounts of retinal scattering. The values were 2.04, 1.42, and 1.49 for subjects NL, CG, and PA, respectively.

C. Ocular Modulation Transfer Functions

We computed the single-pass MTF with the calculation procedure outlined above from the double-pass images obtained with high magnification and equal-size entrance and exit pupil diameters. Eliminating the dc peak in the MTF is equivalent to subtracting a constant value from the double-pass image before computing the Fourier transformation. The visible double-pass image appears quite constant from approximately 0.5 deg (see Fig. 7), and then the above-mentioned procedure clearly seems appropriate. However, since the near-infrared double-pass images continue to decrease at higher angles, subtracting a constant did not appear to be the best procedure. Instead, we first fitted an exponential function to the tail of the infrared double-pass images (beyond 15 arcmin of the radial profiles of the double-pass infrared

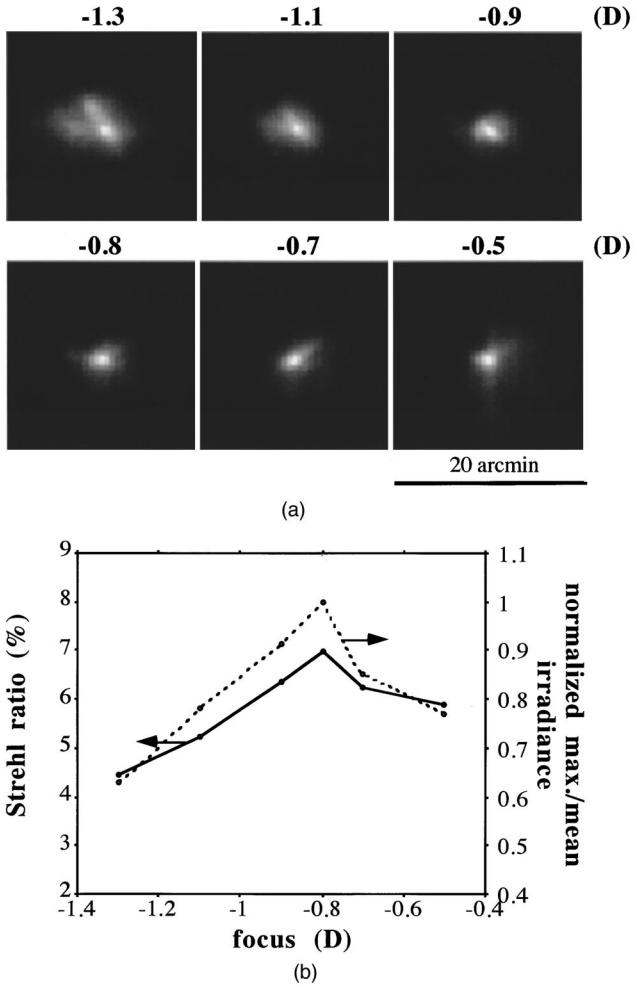

Fig. 5. (a) Double-pass aerial images for observer CG in different foci with near-infrared light and 4-mm pupil diameter in both passes. (b) Two different image-quality criteria used to select the best image: the Strehl ratio (solid curve) and the normalized maximum divided by the mean irradiance (dashed curve) as a function of focus.

Table 1. Doubles Pass (Obj.) and Subjective (Subj.) Best-Focus Settings (in Diopters) and Their Difference (Δ)

	Subject				
Focus	NL1	NL2	NL3	CG	PA
Green (543 nm)					
Obj. (±0.05)	−4.30	−4.35	−4.35	−1.80	−2.25
Subj. (±0.05)	−4.22	−4.30	−4.30	−1.80	−2.60
Δ	−0.08	−0.05	−0.05	0	0.35
Near infrared (780 nm)					
Obj. (±0.05)	−3.30	−3.35	−3.45	−0.80	−1.35
Subj. (±0.05)	−3.28	−3.34	−3.34	−0.83	−1.42
Δ	−0.02	0.01	−0.11	0.03	0.07
OLCA (±0.1)[a]	1.0	1.0	0.9	1.0	0.9
SLCA (±0.1)	0.9	1.0	1.0	1.0	1.2

[a] OLCA and SLCA represent the chromatic difference in focus obtained from the double pass and the subjective focus, respectively.

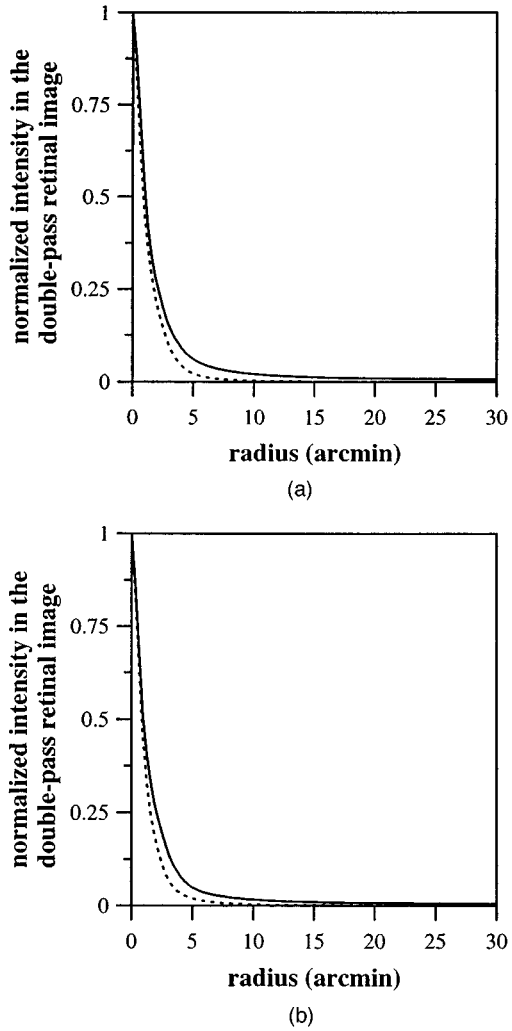

Fig. 6. Radial profiles of the normalized intensity in the double-pass retinal images obtained with 4-mm pupil diameter for subjects (a) NL and (b) PA with near-infrared (solid curve) and green (dashed curve) light.

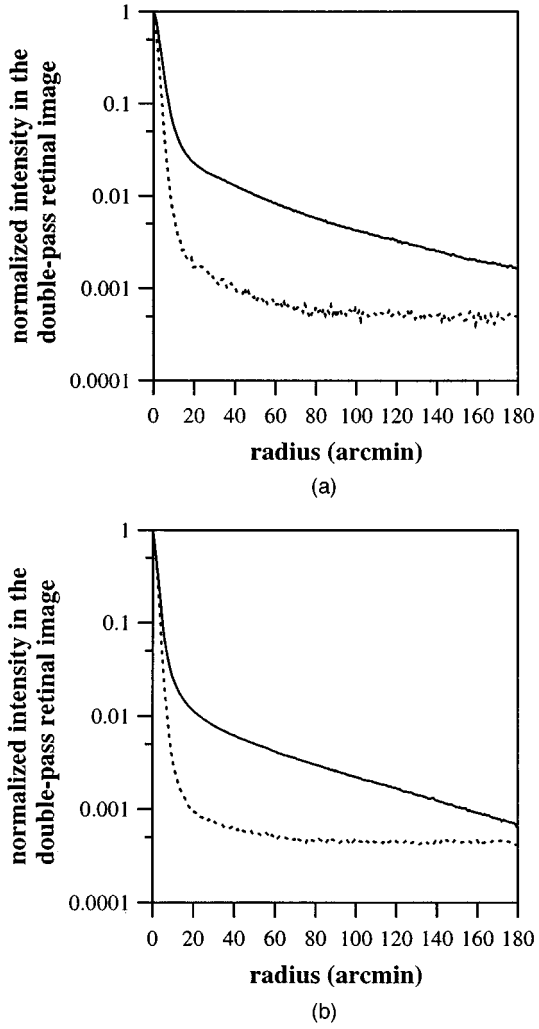

Fig. 7. Radial profiles of the normalized intensity in the double-pass retinal images in a logarithm scale for a large (3 deg) semi-field of view. Solid and dashed curves correspond to near-infrared and green light, respectively, obtained for subjects (a) NL and (b) PA when images obtained with 4-mm pupil diameter were used.

images). Second, we subtracted this exponential function from the double-pass image and renormalized the image. Finally, we computed the Fourier transformation. Figure 8 presents an example. In Fig. 8(a) the normalized infrared image is shown before (solid curve) and after (long-dashed curve) subtracting the exponential function (near-horizontal dashed curve); it is compared with the green retinal image (short-dashed curve) up to 0.1 in the intensity scale. In Figure 8(b) the computed MTF's from both the original infrared image (solid curve) and the infrared image after the exponential background subtraction (dashed curve) are presented. In both cases we used the complete calculation scheme described in Subsection 2.C. In practical terms, as can be noted from Fig. 8(b), there are very small differences in the resulting MTF's. Although it seems more elegant to subtract the exponential to remove the scattering halo in the infrared images, we tested the efficacy of performing the same procedure in both the green and the near-infrared images to compute the MTF's. That is, we subtracted a constant instead of an exponential function from the infrared double-pass images. One-dimensional MTF results, obtained by averaging the resulting two-dimensional MTF's across every orientation, for green and near-infrared and two subjects, are presented in Fig. 9. In every subject the infrared MTF's were lower than the green MTF's. However, if the MTF's are represented against their normalized spatial frequency to the diffraction limit for each wavelength, the resulting MTF's are quite similar for both wavelengths. These MTF's are presented in Fig. 10. By using this representation, we show the MTF results approximately as if they had the same wavelength or were collected with an effective pupil diameter to yield the same diffraction-limit cutoff in each case.

It should be noted here that the goal of this procedure is to use the central cores of the near-infrared double-pass images to predict the green MTF. Then, by subtracting the higher halo in the infrared images, we eliminate the factors that occur mainly in the near infrared.

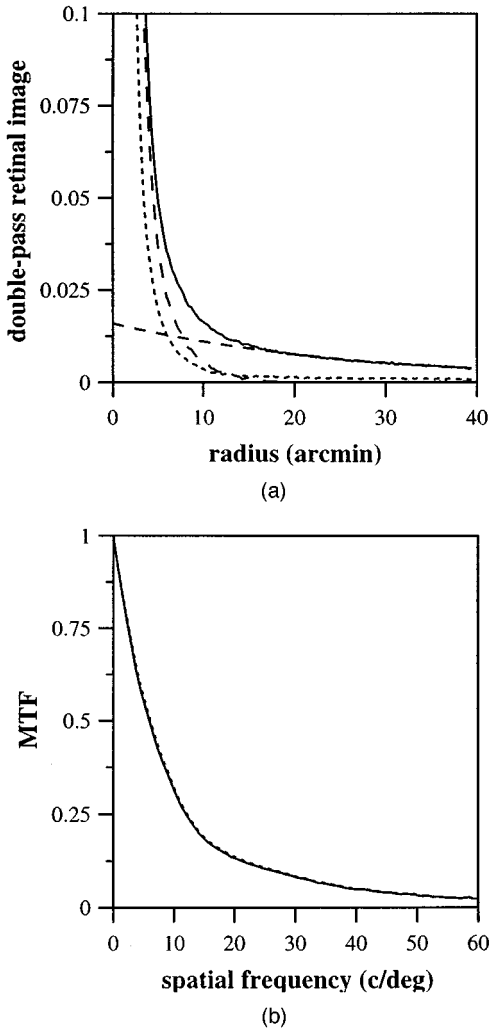

Fig. 8. Detail of radial profiles of the normalized intensity in the double-pass retinal images of PA. Near-infrared (solid curve), exponential curve adjusted (near-horizontal dashed curve), subtraction of exponential from near-infrared (long-dashed curve), and results recorded with green light (short-dashed curve). (b) Near-infrared MTF's for PA calculated from the same double-pass image after subtraction of an appropriate constant background (solid curve) and the two-dimensional exponential adjusted in (a).

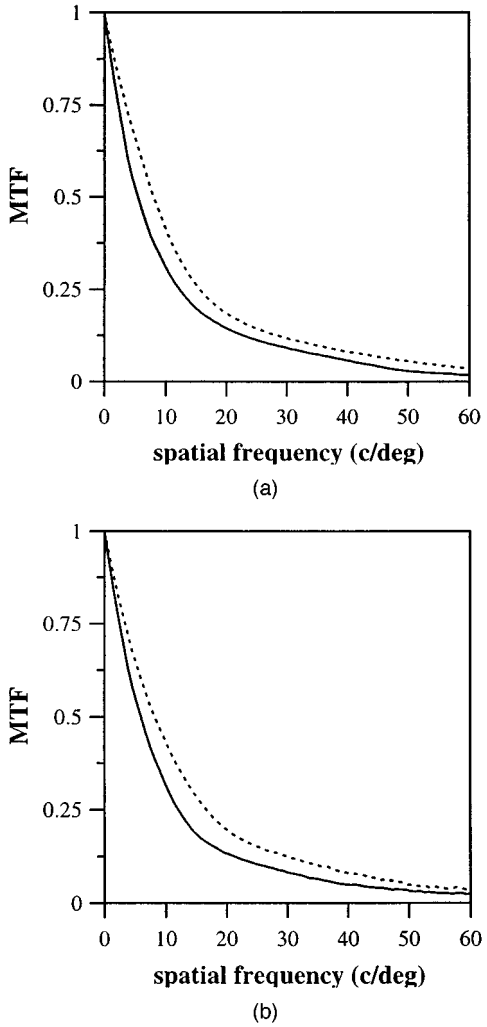

Fig. 9. MTF's calculated from double-pass images for subjects (a) NL and (b) PA with near-infrared (solid curves) and green (dashed curves) light when 4-mm pupil diameter was used.

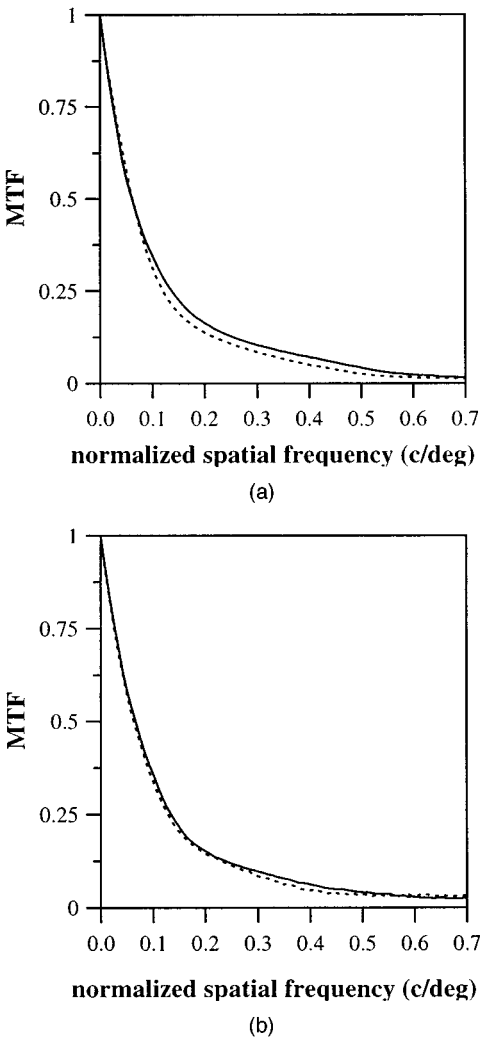

Fig. 10. Same MTF results as in Fig. 9 represented versus the normalized spatial frequency (divided by the cutoff spatial frequency for the diffraction-limited case). Solid and dashed curves correspond to near-infrared and green light, respectively.

D. Double-Pass Images with Unequal Entrance and Exit Pupil Diameters

Odd aberrations are canceled in the double-pass images obtained with equal-size entrance and exit pupils, although the MTF is correctly computed.[12] The use of an asymmetric configuration in the double-pass apparatus with unequal entrance and exit pupil diameter permits us to obtain information on the odd asymmetric aberrations.[10] We show here that this method can also be used with infrared illumination. Figures 11 and 12 show the results for subjects NL and PA in near-infrared (top) and green (bottom) light, respectively. The images are represented both as gray-level images and as contour lines. Every image was collected at best focus with a 1.5-mm-diameter stop for the first passage and a 6-mm-diameter stop in the second passage. For both wavelengths the asymmetries in the retinal images are captured, despite the larger background in the infrared. The symmetry of the filtered infrared beam appears good enough to render the correct asymmetric ocular aberrations. Although the effective first-pass and second-pass stops are not equal for the two wavelengths, it can be seen qualitatively that the infrared images are broader (owing to the scattering on the retina) and that the asymmetry present in the green images also appears in the infrared ones.

4. DISCUSSION

The two main goals in this study were to measure the retinal spread function in the near infrared and to evaluate the possibilities of using this wavelength to estimate the optical performance of the eye in the visible range with the double-pass method. To do this, we built an infrared double-pass apparatus to record near-infrared retinal images. We also estimated the approximate location of the retinal reflection plane for near-infrared light with respect to the subjective focal plane assumed to lie at the external limiting membrane. We used as a reference the double-pass results obtained in green light under conditions the same as those for the infrared results. Several previous studies showed the validity of double-pass estimates of image quality obtained in visible light.[6,12,14] It was also shown that the location of the retinal reflection in visible light, estimated by comparison of subjective and double-pass best focus, was close to the cone inner segment layer. It is also believed that the ocular MTF obtained by the double-pass method is a better estimate in green than in red light.[6] In the first series of experiments, we compared the subjective and double-pass best focus both for green and for near-infrared light. In both cases we found a close agreement between the focus settings, extending the previous finding for visible light[6] to the near-infrared range. This suggests that most of the light of the central cores of the double-pass images comes from a layer close to the photoreceptors. This is an important result for automatic refractor devices for which critical assumptions are usually made concerning the possible plane for retinal reflection. On the other hand, the large tails in the infrared image can explain why in infrared fundus imaging quite blurred images are usually obtained with nonconfocal devices. The experiments that compared subjective and double-pass best focus were carried out with paralyzed accommodation, with use of tropycamide. We repeated the whole set of measurements in one subject (NL2), using cyclopentholate instead of tropycamide, and obtained the same results. This assured us that there were no effects of an incorrectly paralyzed accommodation on the focus results. One of the reasons to use 780-nm wavelength is that it is slightly visible at safe levels of illumination, allowing us to perform subjective measurements. The chromatic difference of focus found between 543 and 780 nm was ~1D in all the subjects (see Table 1). This is a result similar to that expected from extrapolating to 780 nm previous measurements of longitudinal chromatic aberration.[15,16]

The near-infrared double-pass best images (shown in Figs. 6 and 7) present a higher intensity in the tails than to the green images, which is probably due to the larger retinal scattering for the infrared. For instance, in subject NL, while the relative intensity to the maximum at 1 deg is less than 0.001 for the green light, its ~0.01 for the infrared. This difference is approximately the same for

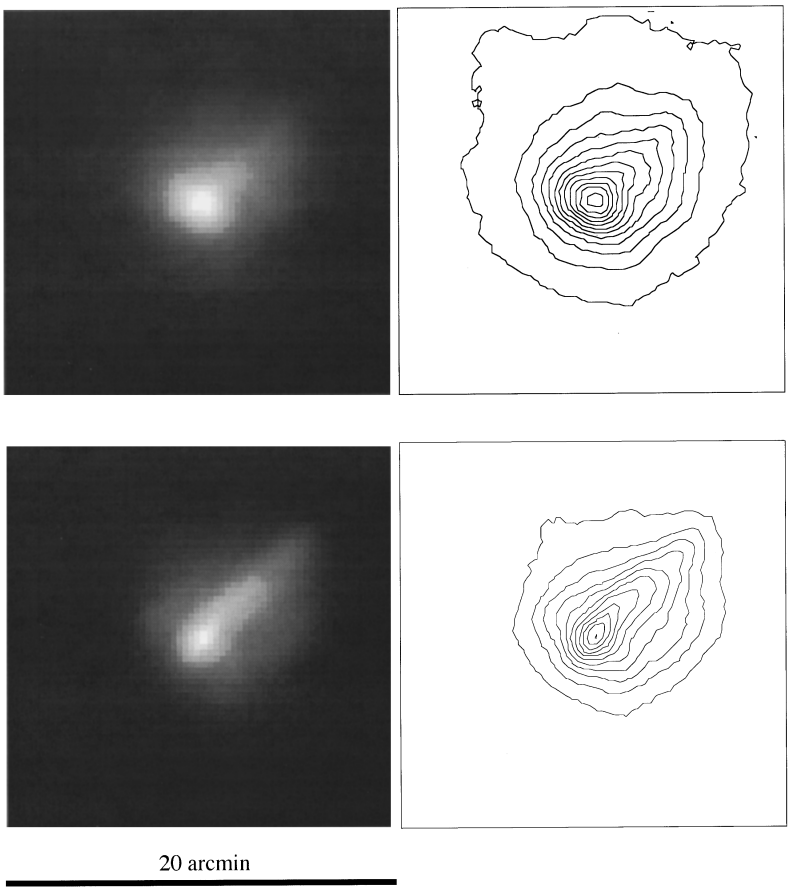

Fig. 11. Gray-level and contour plots for near-infrared (top) and green (bottom) retinal images recorded with unequal first- (1.5-mm) and second-pass (6-mm) stops for subject NL. These double-pass images contain information on ocular asymmetric aberrations. Note that the two images have roughly the same shape.

all the subjects tested. However, and this is the main difference from previous studies on the infrared spread function,[1] the width at half-height in double-pass images is quite similar in green and infrared light: ~2–3 arcmin. These results are in agreement with calculations of the shape of the retinal spread that is due to scattering in the ocular fundus for visible and near-infrared light.[17] A recent report[18] using longer infrared wavelengths showed a much larger retinal spread function. This could indicate that longer infrared wavelengths can spread farther. Nevertheless, more experiments of this type should be carried out with infrared wavelengths longer than 780 nm, which are of interest in different ophthalmic instrumentation.

Low- and mid-order aberrations are the main contributors to the spread in the image at shorter distances (the central core), and higher-order aberration and scattering contribute mostly to the intensity in the image tails (the background of the image). We followed the conventional way of not considering the scattering in the MTF, by eliminating the effect of the scattering halo as described in Subsection 2.C and normalizing the MTF to 1. Then, since the spreads of the central cores in the images are similar for the two wavelengths, it is not surprising that the MTF results also appear similar for the two wavelengths. If, as in Fig. 10, the MTF is represented in a spatial-frequency scale normalized to the diffraction-limited value to compensate somewhat for the different relative contributions of the diffraction for each wavelength, the differences in the MTF's practically disappear. In addition, we showed that using infrared illumination in the asymmetric double-pass apparatus allows us to capture roughly the same asymmetric aberrations of the eye as are obtained when green light is used.

To our knowledge, near-infrared light has not been used before in the double-pass technique, despite some technical advantages, such as the higher retinal reflection factor for larger wavelengths[7] and the better sensitivity of most detectors and imaging devices in the near infrared. On the contrary, several difficulties limit the use of near infrared in the double pass. In particular, the larger retinal scattering for the infrared should produce broader double-pass retinal images that could in principle underestimate the MTF, and there are experimental difficulties involved in the use of near infrared, such as aligning the system and keeping the safety conditions under control. The similar MTF results obtained in green and in infrared light when the chromatic difference of focus is well corrected, indicates the possibility of using the double-pass apparatus with infrared illumination. This presents interesting advantages: permitting measurement of the optical performance of the eye under natural viewing, allowing, for instance, further evaluation of the relationship between aberrations and ocular accom-

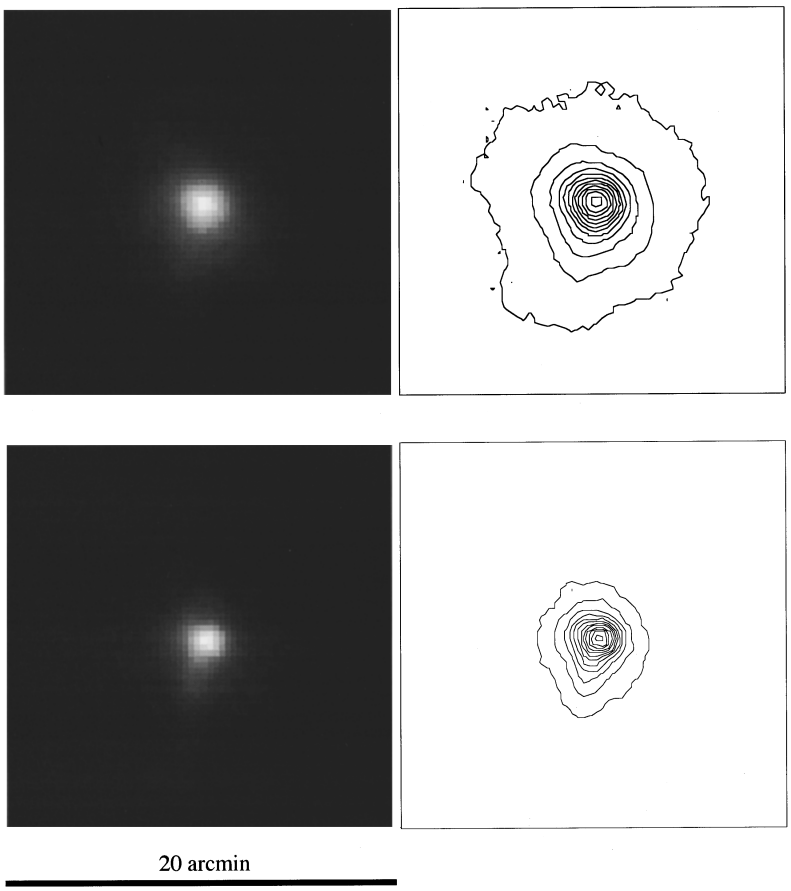

Fig. 12. Gray-level and contour plots for near-infrared (top) and green (bottom) retinal images recorded with unequal first- (1.5-mm) and second-pass (6-mm) stops for subject PA. These double-pass images contain information on ocular asymmetric aberrations. Note that the two images have roughly the same shape.

modation,[19] and opening the possibility of the use of the double pass as a clinical instrument for testing ocular performance under a variety of situations that are comfortable for the subject.

ACKNOWLEDGMENTS

This research was supported by Dirección General de Investigación Cientifica y Técnica (Spain) grant PB94-1138-C02-01. We thank Joaquín Campos from Instituto de Física Aplicada, Consejo Superior de Investigaciones Cientificas (Madrid), for the emission spectrum measurement of the diode laser and C. González for serving as a subject.

Address correspondence to Pablo Artal at the address on the title page; e-mail: pablo@fcu.um.es.

REFERENCES

1. T. N. Cornsweet and H. D. Crane, "Servo-controlled infrared optometer," J. Opt. Soc. Am. **60**, 548–554 (1970).
2. F. Schaeffel, L. Farkas, and H. C. Howland, "Infrared photoretinoscope," Appl. Opt. **28**, 1505–1509 (1989).
3. A. E. Elsner, S. A. Burns, J. J. Weiter, and F. C. Delori, "Infrared imaging of sub-retinal structures in the human ocular fundus," Vision Res. **36**, 191–205 (1996).
4. D. Huang, E. A. Swanson, C. P. Lin, J. S. Schuman, W. G. Stinson, W. Chang, M. R. Hee, T. Flotte, K. Gregory, C. A. Puliafito, and J. G. Fujimoto, "Optical coherence tomography," Science **254**, 1178–1181 (1991).
5. A. F. Fercher, C. K. Hitzenberger, W. Drexler, G. Kamp, and H. Sattman, "In vivo optical coherence tomography," Am. J. Ophthalmol. **116**, 113–114 (1993).
6. D. R. Williams, D. Brainard, M. MacHahon, and R. Navarro, "Double-pass and interferometric measures of the optical quality of the eye," J. Opt. Soc. Am. A **11**, 3123–3135 (1994).
7. F. C. Delori and K. P. Pflibsen, "Spectral reflectance of the human ocular fundus," Appl. Opt. **28**, 1061–1077 (1989).
8. J. Santamaría, P. Artal, and J. Bescos, "Determination of the point-spread function of human eyes using a hybrid optical–digital method," J. Opt. Soc. Am. A **4**, 1109–1114 (1987).
9. P. Artal and R. Navarro, "Monochromatic modulation transfer function of the human eye for different pupil diameters: an analytical expression," J. Opt. Soc. Am. A **11**, 246–253 (1994).
10. P. Artal, I. Iglesias, N. López-Gil, and D. G. Green, "Double-pass measurements of the retinal-image quality with unequal entrance and exit pupil sizes and the reversibility of the eye's optical system," J. Opt. Soc. Am. A **12**, 2358–2366 (1995).
11. W. J. Smith, *Modern Optical Engineering. The Design of Optical Systems*, 2nd ed. (McGraw-Hill, New York, 1990).
12. P. Artal, S. Marcos, R. Navarro, and D. R. Williams, "Odd aberrations and double-pass measurements of retinal image quality," J. Opt. Soc. Am. A **12**, 195–201 (1995).
13. D. R. Williams, P. Artal, R. Navarro, M. J. McMahon, and D. H. Brainard, "Off-axis optical quality and retinal sampling in the human eye," Vision Res. **36**, 1103–1114 (1996).
14. P. Artal and R. Navarro, "Simultaneous measurement of

two-point-spread functions at different locations across the human fovea," Appl. Opt. **31**, 3646–3656 (1992).
15. W. N. Charman and J. A. M. Jennings, "Objective measurements of the longitudinal chromatic aberration of the human eye," Vision Res. **16**, 999–1005 (1975).
16. P. A. Howarth and A. Bradley, "The longitudinal chromatic aberration of the eye and its correction," Vision Res. **26**, 361–366 (1986).
17. I. J. Hodgkinson, P. B. Greer, and A. C. B. Molteno, "Point-spread function for light scattered in the human ocular fundus," J. Opt. Soc. Am. A **11**, 479–486 (1994).
18. D. D. Saunders and H. C. Howland, "Measurement of the infrared line and point spreads in the human eye," Invest. Ophthalmol. Vis. Sci. (Suppl.) **37**, S720 (1996).
19. P. Artal and N. López-Gil, "Monochromatic retinal image quality as a function of accommodation," Invest. Ophthalmol. Vis. Sci. (Suppl.) **37**, S719 (1996).